A robust retrieval of water vapor column in dry Arctic conditions using the rotating shadowband spectroradiometer

P. Kiedron,[1] J. Michalsky,[1] B. Schmid,[2] D. Slater,[3] J. Berndt,[1] L. Harrison,[1] P. Racette,[4] E. Westwater,[5] and Y. Han[5]

[1] Atmospheric Sciences Research Center, State University of New York, Albany, New York, USA.

[2]Bay Area Environmental Research Institute, San Francisco, California, USA.

[3]Pacific Northwest National Laboratory, Richland, Washington, USA.

[4]NASA Goddard Space Flight Center, Greenbelt, Maryland, USA.

[5]Cooperative Institute for Research in Environmental Sciences, University of Colorado and National Oceanic and Atmospheric Administration, Boulder, Colorado, USA.

Abstract. A method to retrieve water vapor column using the 940-nm water vapor absorption band in dry Arctic conditions is presented. The retrievals with this method are stable with respect to uncertainties in instrument radiometric calibration, air pressure, solar source function, and aerosols. The water vapor column was retrieved with this method using spectra obtained with the rotating shadowband spectroradiometer (RSS) that was deployed during an intensive observation period near Barrow, Alaska, in March 1999. A line-by-line radiative transfer model was used to compute water vapor transmittance. The retrievals with this method are compared with retrievals obtained from three independent measurements with microwave radiometers. All four measurements show the same pattern of temporal variations. The RSS results agree most closely with retrievals obtained with the millimeter-wave imaging radiometer (MIR) at its 183 GHz ± 7 double-side band channel. Their correlation over a period of 7 days when water vapor column varied between 0.75 mm and 3.6 mm (according to RSS) is 0.968 with MIR readings 0.12 mm higher on average.

1. Introduction

The primary window through which infrared radiation escapes from the lower atmosphere is around 10 μm. However, in the Arctic regions the winter atmosphere can be very dry; total column water vapor can be a few millimeters or even less than 1 mm. This allows a secondary atmospheric window around 20 μm to open. The magnitude of this effect depends critically on the amount of water vapor. Typically, the measurement of water vapor profile is made by radiosondes. These measurements of relative humidity tend to be problematic in very dry environments such as the Arctic [*Wade*, 1994]. Alternatively, microwave radiometers are used to determine water vapor column more accurately.

Infrared radiation model validation critically depends on the accuracy of the model inputs. In the Atmospheric Radiation Measurement (ARM) program [*Stokes and Schwartz*, 1994] there has been an emphasis on the specification of the distribution of water vapor with altitude as well as on the total column water. *Clough et al.* [1996] demonstrated that infrared models that use radiosonde water vapor profiles that are scaled to give the same total column water vapor as the microwave radiometer gave better agreement with infrared measurements than radiosonde humidity measurements without scaling. As an example, *Liljegren and Lesht* [1996] found that column water vapor from Vaisala RS-80 radiosondes is commonly dry relative to the ARM operational microwave radiometer that operates in north central Oklahoma; *Westwater et al.* [2000a] arrived at a similar conclusion in the tropics. Both cases are concerned with relatively high water vapor amounts. *Lesht* [1999] developed a correction for the dry bias; however, in the dry cold environments, the issue is more the lack of sensitivity to moisture.

In this paper we present an independent method for determining the total amount of water vapor from direct solar spectral irradiance in the near infrared. This method depends primarily on the water vapor absorption model that is used in HITRAN and is tied to laboratory measurements of water vapor absorption. This can provide an accurate measurement of water vapor along the path in the direction of the Sun for direct shortwave radiation modeling. Microwave radiometers can operate in a zenith-pointing mode except during calibration, but they cannot point in the direction of the Sun. Therefore to compare retrievals from a sun photometer such as the rotating shadowband spectroradiometer (RSS) [*Harrison et al.*, 1999] with those from microwave radiometers, the water vapor amount in the direction of the Sun must be

properly scaled by air mass to derive the vertical water vapor column. The correctness of scaling hinges on the validity of the assumption that the water column profile is spatially and temporally homogeneous and on some knowledge of the relative water column profile. One should bear in mind that balloon-borne radiosondes sample along a path governed by the winds and do not represent the true water path in the direction of either the sun or the zenith. Thus the knowledge of the actual water column profile that is needed for the scaling is often limited.

Currently, the water vapor column is measured by microwave radiometers (MWR) [*Liljegren*, 2000] continuously deployed by the ARM program at all of its cloud and radiation test bed (CART) sites [*Stokes and Schwartz*, 1994]. The MWR operates at 23.8 and 31.4 GHz. For low values of water vapor such as those experienced in the Arctic, the signal at the MWR frequencies is very low. Consequently, the retrievals from the MWR are more affected by radiometric noise and calibration errors than when the measurements are made at warmer, more humid locations. Theoretically, a stronger line, such as at 183 GHz, should yield a better signal-to-noise ratio in dry atmospheres. Developing improved techniques for measuring water vapor column in the Arctic was the motivation for the intensive observation period that was conducted during the late winter and early spring of 1999 at the North Slope of Alaska (NSA) ARM site near Barrow, Alaska [*Racette et al.* 2000].

The RSS, deployed by the Atmospheric Sciences Research Center (ASRC), was the only Sun photometer taking part in this experiment. In addition to the MWR, NOAA Environmental Technology Laboratory (ETL) and NASA Goddard Space Flight Center (GSFC) deployed microwave radiometers spanning 25 channels between 21 GHz and 340 GHz. Measurements near the 183 GHz absorption line were made by two independently calibrated instruments. This line is about 100 times stronger than the 22.235 GHz line more commonly used for water vapor remote sensing. The millimeter-wave imaging radiometer (MIR) from GSFC operated with seven channels 89, 150, 183 ± 1, 183 ± 3, 183 ± 7, 220, and 340 GHz [*Racette et al.*, 1996]. The circularly scanning radiometer (CSR) from NOAA ETL operated with 12 channels: 20.6, 31.65, 183 ± 0.5 183 ± 1, 183 ± 3, 183 ± 7, 183 ± 12, 183 ± 15, 325 ± 1, 325 ± 3, 325 ± 8, and 340 GHz. The plus-or-minus notation refers to the offset from the center frequency of the channel that uses double-side-band detection.

In late winter Arctic conditions the amount of water vapor can be small, often below 2 mm in a vertical column when temperatures are extremely low and the skies are clear. For this reason, emission from the strong channels near 183 GHz was measured with the MIR and the CSR and compared with measurements from the standard weaker microwave absorption channels at 23.8 GHz and 31.4 GHz of the MWR [*Racette et al.*, 2000]. The retrievals from the RSS use the 940-nm band which is the strongest water vapor absorption band within the RSS spectral range of 380 - 1050 nm.

The RSS provides continuous direct irradiance spectra over 512 pixels covering the wavelengths 350 – 1080 nm. Unlike filter radiometers [*Schmid et al.*, 1996; *Ingold et al.*, 2000] that use a single channel to sample a water vapor band, the continuous spectra offer an opportunity to over sample and produce a more robust retrieval. The procedure described in the next section uses a baseline removal method that unlike the differential (or ratio) technique used by *Michalsky et al.* [2001], anchors the baseline at two continuum points on either side of the absorption band. The advantage of this method is that the explicit knowledge of aerosol optical depth is not required. Similar baseline removal techniques in water vapor retrieval were used by *Gao and Goetz* [1990] to eliminate soil reflectance from airborne spectrometer data and by *Thome et al.* [1992] in the three-channel solar radiometer to remove aerosol optical depth. In section 3 we discuss the air mass scaling (and associated errors) that is necessary to convert the total water vapor in the direction of the Sun to the vertical column. Next we describe the absorption model used to generate transmittance spectra for comparisons with the RSS data. In section 5 we present retrieval results and compare them with results from the MWR and MIR. In section 6 we discuss errors associated with the RSS measurements. Finally, we show analysis results to support our claim of the robustness of the method.

2. Method Description

The water vapor is computed by matching the water vapor transmittance obtained from measurement with the water vapor transmittance obtained from a model. First we describe our method of obtaining the water vapor transmittance from the RSS. The direct irradiance that the RSS measures every minute at pixels p=0,…,511 is divided by the extraterrestrial irradiance and the Rayleigh transmittance:

$$I(p) = \frac{I_{RSS}(p)}{I_{ET}(p)T_{Rayleigh}(p)}, \qquad (1)$$

where the extraterrestrial irradiance $I_{ET}(p)$ is at the RSS resolution. The resulting normalized irradiance $I(p)$ still contains extinction due to components other than water vapor (such as other gases, aerosols, and thin clouds), which are not being retrieved explicitly in this method. Their influence on the retrieval is removed by dividing $I(p)$ by the baseline irradiance

$$I_0(p) = I(p_1)\left(\frac{I(p_2)}{I(p_1)}\right)^{\frac{\lambda-\lambda_1}{\lambda_2-\lambda_1}}. \qquad (2)$$

The baseline irradiance (2) can be thought of as a normalized irradiance without water present as long as its anchor pixels p_1 and p_2 are where the water absorption is small (see Figure 1). Then for pixels $p_1<p<p_2$ we calculate the RSS water vapor transmittance

$$T_{RSS}(p) = I(p)/I_0(p). \quad (3)$$

Formula (2) is an exponential interpolation of irradiance that is equivalent to linear interpolation of optical depth in the wavelength space. We note that other interpolating formulas can be used, such as linear interpolation of irradiance or interpolation in pixel or wave number space instead of the wavelength space. For instance, *Thome et al.* [1992] used linear interpolation of the logarithm of aerosol optical depth. However, simulations that we performed indicate that the interpolation in (2) results in slightly more robust retrievals.

The model transmittance at RSS resolution is calculated as an average of the high-resolution transmittance from a model $t(w,\lambda)$, where w is water vapor in the direction of the Sun, weighted by the RSS pixel function $s(p,\lambda)$:

$$T(w,p) = \frac{\int t(w,\lambda)s(p,\lambda)d\lambda}{\int s(p,\lambda)d\lambda}. \quad (4)$$

To replicate the process of obtaining RSS transmittance and thus eliminate small effects of water absorption at the anchor points p_1 and p_2, the model transmittance must be normalized by its baseline:

$$T_o(w,p) = T(w,p_1)\left(\frac{T(w,p_2)}{T(w,p_1)}\right)^{\frac{\lambda-\lambda_1}{\lambda_2-\lambda_1}}. \quad (5)$$

This results in the model transmittance that is equivalent to the RSS transmittance given by (3)

$$T_{\mathrm{mod}}(w,p) = T(w,p)/T_0(w,p). \quad (6)$$

The water vapor column is retrieved by perturbing *w* until

$$T_{\mathrm{mod}}(w,p) = T_{RSS}(p) \quad (7)$$

at a particular pixel *p*. In all retrievals in this paper we set *p*=455, that is, at approximately 940 nm where the absorption is the largest, p_1=441 (883 nm) for the short wavelength anchor point, and p_2= 469 (1000 nm) for the long wavelength anchor point. We emphasize that for conditions with greater water vapor amounts, using the weaker water bands near 725 nm and 820 nm may be preferred to avoid the very low transmittance of the 940-nm band in these circumstances.

Small wavelength shifts are possible during the operation of RSS because of temperature effects. Further, the absolute wavelength errors associated with the RSS wavelength calibration may propagate into the pixel functions $s(p,\lambda)$. Also, wavelength scale errors are possible in the model. Consequently, we also performed retrievals using a least square fit with respect to pixel shift Δp and water column *w*:

$$\min_{w,\Delta p}\sum_p [T_{RSS}(p) - T_{\mathrm{mod}}(w, p+\Delta p)]^2, \quad (8)$$

where $T_{\mathrm{mod}}(w,p+\Delta p)$ is obtained from $T_{\mathrm{mod}}(w,p)$ by means of cubic spline interpolation. In all retrievals the summation (8) was carried out over only three pixels 454, 455, and 456 near the strongest absorption feature of the 940-nm band. The values of Δp obtained from (8) serve as an estimate of wavelength stability and/or accuracy, and the difference between water vapor *w* obtained from formula (7) and from formula (8) gives us a measure of wavelength-related error.

3. Scaling to Vertical Column

The total water vapor *w* in the direction of the Sun is scaled to the vertical water column using

$$h = w/m_{water}, \quad (9)$$

where m_{water} is the water vapor air mass. The water vapor air mass is calculated assuming standard temperature and water vapor profiles using the analytical approximation

$$m_{water} = (\sin(\eta) + 0.0548(2.650+\eta)^{-1.452})^{-1}, \quad (10)$$

where η is Sun elevation angle, which was derived by *Kasten* [1965]. The approximation of (10) means that the water vapor column derived from (9) is less accurate than the value of water vapor in the direction of the Sun from (7) or (8). The water vapor air mass depends explicitly on the form of the water column profile, which is not known exactly. However, this error is negligible for small air masses because all water mass formulas, regardless of the shape of the water column profile, converge at low air masses. We try to estimate this error using profiles from balloon radiosondes. Radiosonde launches coincided with 8 days out of 11 days when RSS retrievals were possible. From these profiles, water vapor air mass was calculated by integrating the optical path (see equation (2) of *Schotland and Lea* [1986]). The results were compared with values produced by (10). The results that are presented in Figure 2 indicate that (10) overestimates water vapor air mass by up to 3% within air mass ranges where retrievals were performed. If we could assume that the radiosonde data represent true water column profiles and that the shape of the profiles remained stable during each day, then we could use true water air mass instead of (10). Unfortunately, the validity of such an assumption is questionable. Figure 2 allows us to conclude that we may have underestimated the total water vapor in the vertical, but by no more than 3% even for the larger air masses used.

4. Model Definition

We used version 5.21 of the line-by-line radiative transfer model (LBLRTM) [*Clough et al.*, 1996] to create a lookup table of $T(w, p)$ (see (4)). The LBLRTM 5.21 uses the HITRAN-96 [*Rothman et al.*, 1998] spectroscopic database but includes the corrections for water vapor lines in the visible and near infrared as suggested by *Giver et al.* [2000]. The LBLRTM was run in its transmittance mode (considering only water vapor line and continuum absorption) over the spectral range covered by the response function of the specific RSS pixels. We performed the computations using the built-in subarctic winter atmosphere (Pw=4.2 mm) and a drier (Pw=2.2 mm) user-defined model atmosphere. The altitude in the simulations was set to sea level according to our observation site. The solar zenith angle (SZA) was varied in the range from 0° to 80° at steps of 5° for SZA≤50° and 2.5° for 50°≤SZA≤85°. These settings produced slant path water vapor amounts ranging from 2.2 mm to 46 mm.

5. Results

In Figure 1, model transmittances obtained from the two methods implied by (7) and (8) are compared with measured transmittances for two different air masses m=2.10 and m=16.41. The ratio of transmittances shows that the match between experimental and model transmittances is very good and for the larger air masses formula (8) yields slightly better agreement.

Plate 1 shows a comparison of the vertical water vapor column retrieved using the RSS, the MWR, and the MIR 183 ±3, and 183 ±7 GHz channels. The MWR and MIR retrievals are based upon the *Rosenkranz* [1998] model of water vapor and oxygen absorption. The MWR retrievals use both channels of the MWR, whereas the MIR retrievals are made using single channels. The MWR and MIR measure vertical water vapor columns directly. The RSS, on the other hand, scales the water vapor in the solar path by (10) to arrive at the vertical column measurements. Therefore some discrepancy between the results can be attributed to the nonuniformity of water column profiles.

The data presented in Plate 1 cover two periods: March 6-11 (day of year 1999 = 65-70) was characterized by very clear conditions that resulted in low-noise RSS retrievals; five days at the end of March (day of year 1999 = 85-89) were semiclear with hazy conditions that produced significantly higher noise in the retrieved water column by the RSS. The days between the two periods were overcast. According to the MIR and MWR that provided data continuously during the intermediate period, the vertical water vapor column varied between 2 and 6 mm. While there were brief windows when RSS data were usable during that period, we concentrate on predominantly clear periods when water vapor amounts were lowest.

All the independently derived measurements show the same structure and follow the same overall pattern of increases and decreases. Large correlation coefficients in Table 1 confirm this. However, the offset between the measurements is readily apparent. The greatest difference is between the MWR and the MIR 183 ±3 GHz retrievals. The absolute difference between these two measurements is about 0.5 mm, and the relative difference varies between 20% and 40%. The RSS and MIR 183 ±7 measurements fall between the MWR and the 183±3 GHz measurements and agree more closely with one another, having the greatest correlation coefficient. During the first period, the RSS measures about 0.1 mm or approximately 5% lower than the MIR 183±7 measurements. During the second period the agreement is even better, but RSS measurements indicate, on average, 0.12 mm lower water vapor amounts.

Though the RSS retrieval tracks closely with the other three retrievals, deviations exist in the RSS trend. Near day 85.1 and day 86.1 the RSS measurements decrease more rapidly than the other three measurements. The difference in trends during these periods is attributed to inhomogeneity of the atmosphere and the conversion of the RSS measurement to the vertical column (see (9) and (10)) when using low Sun elevation angles. However, inhomogeneity and conversion to vertical column cannot explain the apparent drift in measurements between the RSS and the MIR 183 ±7 GHz. In the following sections we show that there is no plausible instability in the RSS retrieval to account for this drift, at least in terms of the total water vapor in the direction of the Sun.

We cannot present an unequivocal explanation as to why the RSS and MIR 183±7 GHz agree the best of all the measurements compared, and agree better during the second period. However, there are two significant sources of error that contribute to the observed differences in the microwave retrievals [*Racette et al.*, 2000]. One source of error is in the calibration of the measured brightness temperature. Calibration measurements using blackbody absorbers and comparisons of the measurements made with independently calibrated measurements of the CSR suggest the brightness temperature accuracy of the MIR 183±3 GHz and 183±7 GHz channels is approximately 3K, which translates to 0.4 mm and 0.8 mm, respectively. The second source of error comes from the absorption model used in the retrieval. Differences in contemporary absorption models can attribute comparable differences in retrieved water vapor column [*Westwater et al.*, 2000b]. The combination of calibration error and errors in the absorption models is believed to account for the differences observed in the microwave measurements. Plate 1 also contains results from seven radiosonde launches. The moisture data were corrected with the *Lesht* [1999] procedure by *Racette et al.* [2000]. At this point we cannot explain why radiosonde data agree the best with MWR retrievals on

days 68, 69, and 70 and agree the best with RSS and MIR 187±7 retrievals on days 87, 88, and 89, and the results on day 86 overestimate all other retrievals.

6. RSS Related Errors

Retrievals on April 14, 1999, were used to evaluate RSS related errors and the method's sensitivity. That day was clear, and observations over a wide range of air masses (from 2 to 16) were possible. In the morning the vertical water column was estimated to be about 1.4 mm, while in the afternoon it climbed to 2.2 mm. The estimates of RSS-related errors are presented in Plate 2. Each curve in the plate consists of morning and afternoon branches that do not necessarily coincide. The error types in this section are discussed in order of their descending importance.

6.1. Stray Light

The slit function of the RSS indicates that the amount of energy transferred from a central wavelength to the far ends of the slit function's wings is less than 10^{-5} [see *Kiedron et al.* 1999, Figure 9]. For this reason the spectrum is slightly distorted and the absorption bands are shallower than if the slit function were zero outside the immediate passband. The consequence of this leak for the water retrieval is the underestimation of water column. The RSS pixel functions were developed using information from slit functions from several laser lines and pixel dependent resolution that was derived from Hg and Cd spectral lamps. The quality of the pixel function was verified when RSS spectra were compared with synthetic spectra, resulting in a very good match [*Mlawer et al.*, 2000]. For this reason we believe that the RSS is sufficiently well-characterized to perform stray light removal using an algorithm akin to the deconvolution method. This algorithm, unlike the method of deconvolution for the purpose of superresolution, is stable as it is concerned with retrieval of low frequencies affected by the wings of the pixel functions. The algorithm removed energy from beyond ±7 pixels from the centers of each pixel function. The retrieved water column increased by 1.5% at low air masses and by up to 3% at large air masses (see Plate 2). We stress the fact that the stray light error is correctable; however, it is time consuming and we did not employ it for the retrievals presented in Plate 1.

6.2. Detection Noise

The detection noise is composed of the readout noise and dark counts and Poisson statistics. The readout noise component was estimated before the deployment of the instrument, and the Poisson component can be deduced from counts. It is possible to get a good estimate of the noise at each pixel for each exposure and subsequently calculate the noise in terms of water column. As could be expected, the detection noise increases for larger air masses and is larger when partial obstruction of the direct beam occurs; however, the increase is not dramatic. This occurs because the RSS automatically maximizes its exposure to utilize the full dynamic range of the detector according to the irradiance level. The detection noise in Plate 2 is for a single measurement cycle that occurs once every minute. The detection noise is random with a zero mean; thus, averaging consecutive measurements increases the signal-to-noise ratio by the square root of the number of samples in the average.

6.3. Wavelength Related Errors

The wavelength-to-pixel assignment, that is, the absolute wavelength calibration accuracy, is better than 1 nm at 940 nm. The spectrograph of the RSS is temperature-stabilized to better than 0.5°C. This implies that temperature-related changes of the fused silica dispersion element may cause wavelength shifts at 940 nm of no more than 0.5 nm. The wavelength shift error in principle is correctable as wavelength shifts can be deduced from the spectrum. For instance, on April 14, 1999, the wavelength shift did not exceed 0.4 nm. However, the confidence in these deductions decreases rapidly for large air masses due to the reduction in the signal-to-noise ratio. The method that uses (8) in principle corrects for wavelength drift and absolute RSS wavelength errors and wavelength inaccuracy, if any, in the model. The difference between a single-pixel-based retrieval using (7) and one using (8) that fits three pixels can serve as a measure of wavelength-related errors. In Plate 2 this error is little more than 1% even for large air masses.

6.4. Radiometric Calibration

The RSS was calibrated four times during its deployment at the NSA site. The resulting four calibrations from four measurements differed by less than 4% in the near-IR region; however, their slopes differed by less. We could not tell whether the differences occurred because there were changes in RSS responsivity or changes in calibrator irradiance. Our simulation showed that responsivity changes could be explained by ±0.3°C temperature change of the detector array that has a wavelength-dependent temperature coefficient of quantum efficiency in the near IR. We could simulate similar variations by assuming ±75°K color temperature change of the lamp calibrator. Anyway, in the worst case, the impact of different response curves on water retrieval was still less than 0.3% (see Plate 2). The low sensitivity to responsivity change demonstrates the robustness of the retrieval method that is attributed to the baseline normalization.

6.5. Timing

The main impact of timing error is on the calculation of actual Sun elevation angle to deduce the water air mass needed from (10). The impact on air mass needed for the

Rayleigh transmittance in (1) is negligible. The RSS computer maintains its time through a network connection to better than 1 s. However, there is some uncertainty related to actual time when the direct irradiance is derived. The RSS does not measure the direct irradiance but derives it from four consecutive measurements during a measurement cycle [*Harrison et al.*, 1994]. The time delays between the four measurements depend on the exposure time, which usually increases from 0.25 s at solar noon to 5 s near dawn and dusk. The delay also depends on the distance that the shadowband needs to travel, which is greater in the afternoon than in the morning. The combination of these delays is significantly smaller that ±30 s. In Plate 2 timing error is estimated to be less than 1% for very large air masses.

6.6. Cosine Correction Error

To derive the direct irradiance, the cosine correction needs to be applied to the measured data [*Harrison et al.*, 1994]. The cosine correction is wavelength (pixel) dependent. The RSS cosine corrections for all pixels were measured prior to deployment at the NSA site using the method described by *Michalsky et al.* [1995]. In fact, this instrument had its cosine corrections measured on three other occasions for prior deployments at the Southern Great Plains (SGP) ARM site. To test the importance of the cosine correction for the retrieval of water, we retrieved water from spectra that were cosine-corrected and spectra that were not cosine-corrected. The difference was less than 0.04% (Plate 2). This is because the relatively small variation of cosine correction between pixels p_1 and p_2 is effectively compensated using baseline normalization.

7. Robustness

Some results presented in Plate 2, mainly the low sensitivity to radiometric calibration errors and cosine correction indicate a high degree of technique robustness that results from normalization by the baseline. Like any ratio method [e.g., *Michalsky et al.*, 2001], this method is invariant to scaling by a constant. Furthermore the interpolating function (2) guarantees invariance to the exponential scaling. It means that the spectrum multiplied by $a\exp[k(\lambda-\lambda_1)/(\lambda_2-\lambda_1)]$ for any values of a and k will yield the same transmittance and, thus, the same water column. In Plate 3 we present results of additional sensitivity studies for the case of April 14, 1999.

7.1. Rayleigh Scaling

To investigate the sensitivity of the method to the pressure errors in the Rayleigh transmittance formula [*Hansen and Travis* 1974],

$$T_{\text{Rayleigh}}(\lambda)=\exp(-0.008569\lambda^{-4}(1+0.0113\lambda^{-2}+0.00013\lambda^{-4})\frac{P}{P_0}m), \quad (11)$$

that is used to normalize measured irradiance in (1), we tested the worst case by comparing two retrievals: one with $P/P_O=1$ and one with $P/P_O=0$. The latter case implies no Rayleigh correction in (1). The difference is less than 1% (see Plate 3). One may conclude that the exact knowledge of air pressure to retrieve water with this method is not necessary.

7.2. Extraterrestrial Normalization

We retrieved water where extraterrestrial irradiance is obtained from the default solar source function (SSF) used in MODTRAN [*Kneizys et al.*, 1996]. Then we retrieved water without normalizing the irradiance in (1) with extraterrestrial irradiance, that is, we assumed $I_{ET}(p)=1$. The difference was smaller than 5% at low air mass and decreased to 1% at large air masses (Plate 3). While we recommend normalizing by extraterrestrial irradiance, we conclude that errors, if any, in the SSF that make it differ from the actual extraterrestrial irradiance should have a negligible effect on water retrieval with this method.

7.3. Linear Scaling

If there is any unaccounted for physical process or error, such as radiometric calibration uncertainties, that tilts the measured irradiance by ±10% between the anchor points the retrieval error will be no more than 0.8% (Plate 3).

7.4. Ångstrom Scaling

Finally, we verify our earlier statement that aerosols do not need to be retrieved explicitly because the baseline normalization diminishes their influence. We assumed an Ångstrom relationship,

$$t_{aer}(\lambda)=\exp(-\beta\lambda^{-\alpha}m), \quad (12)$$

and carried out two retrievals. In either case we multiplied measured irradiance by aerosol transmittance (12) that in the first case had nominal values of β and α and in the second case had β and α changed by ±50% and ±25%, respectively. For Arctic conditions we assumed the value $\beta=0.05$ that resulted in less than 0.3% retrieval error. In the case when aerosols produce much larger optical depth, $\tau(940)=0.53$, the retrieval errors increase but are still below 3% even at large air masses. The interpolating formula (2) minimizes the effects of aerosols but does not eliminate them completely. One can envision a method that is both invariant to scaling by a constant and to the scaling by the Ångstrom formula. Then, however, more than two anchor points are necessary.

8. Summary and Discussion

The deployment and operation of the RSS during the winter experiment was successful. The RSS showed the capability of retrieving total water vapor in the direction of the Sun even at air masses as large as 16 (see Figure 1). The largest error (up to 3%) related to RSS measurement is due to the stray light and could be, but was not, reduced by 1 order of magnitude using a deconvolution algorithm. The signal-to-noise ratio allows one to make measurements at better than 1% precision in 1-min intervals on clear days. The retrieval method is exceptionally robust, which means that it can tolerate a high degree of uncertainty in the actual aerosol content, in the atmospheric pressure, and even in the solar source function. The largest error may be associated with the theoretical calculation of water absorption derived from available models. As Figure 1 shows, the transmittance in the 940-nm band from the LBLRTM 5.21 is consistent with the measured transmittance both for small and large air masses. The same figure cannot tell us whether the relative strength of the band given by the model is correct. If it is, then the retrievals of water column in the direction of Sun with the RSS are accurate to within 3% at the 1-mm vertical water vapor column level. Further improvement is possible with a more sensitive instrument [*Harrison et al.*, 1999] and with the implementation of a stray light correcting algorithm. The discrepancy between the derived vertical water vapor column inferred by the RSS and that obtained by the microwave measurement made by the MWR and MIR may be explained by water profile nonuniformity or by errors in the microwave measurement. If neither is the case, the results from the experiment carried out at the NSA site indicate that the accuracy of the band strength in the 940-nm range in LBLRTM 5.21 is insufficient even after the *Giver et al.* [2000] correction.

After the completion of this paper *Belmiloud et al.* [2000] published experimental results suggesting that the 940-nm water vapor band is stronger by 6% to 10% than that given by *Giver et al.* [2000]. If these experimental results are correct, the amount of water retrieved by RSS would be reduced by 6% to 10%. The correlation coefficients (the second column from the left in Table 1) would not change significantly; however, the differences (the third column) would change. The offsets between the RSS and MWR and MIR±7GHz would be larger and that between the RSS and MIR±3GHz would be reduced. However, more recently the results by *Belmiloud et al.* [2000] at 1130 nm were questioned by *Giver et al.* [2001], implying that the uncertainties in water vapor bands remain unresolved.

A robust algorithm for deriving water vapor in the solar path from RSS measurements has been shown. Comparisons with vertical water vapor column based upon microwave measurements show overall good agreement. Though biases between the measurements exist, comparison in the trends is excellent. The technique shown has application for measuring water vapor column in the Arctic during clear and semiclear sky conditions. The technique is limited to those times when the Sun is above the horizon and visible.

Acknowledgments. The authors would like to thank Mark Beauharnois who helped with the RSS measurements and to Bernie Zak of Sandia National Laboratory and Knute Stamnes of the University of Alaska, Fairbanks, who facilitated the deployment and operation of the RSS at the NSA site. This research was supported by the Environmental Sciences Division of the U.S. Department of Energy through grant DE-FG02-90ER61072 (SUNY) as part of the Atmospheric Radiation Measurement program. Pacific Northwest National Laboratory is operated for the U.S. Department of Energy by Battelle Memorial Institute under contract DE-AC0676RLO 1830. This research was also supported by the Stratospheric Aerosol and Gas Experiment (SAGE III) Science Team, NASA program code 229-10-32-00. Finally, we thank the reviewers for their comments and suggestions that allowed us to improve this paper.

References

Belmiloud, D., R. Schermaul, K.M. Smith, N.F. Zobov, J.W. Brault, R.C.M. Learner, D.A. Newnham, and J. Tennyson, New studies of the visible and near-infrared absorption by water vapor and some problems with the HITRAN database, *Geophys. Res. Lett*., *27*, 3703-3706, 2000.

Clough, S.A., P.D. Brown, J.C. Liljegren, T.R. Shippert, D.D., Turner, R.O. Knuteson, H.E. Revercomb, and W.L. Smith, Implications for atmospheric state specification from the AERI/LBLRTM quality measurement experiment and the MWR/LBLRTM quality measurement experiment, paper presented at ARM Science Team Meeting, Atmos. Radiat. Measure. Program, San Antonio, Tex.,1996.

Gao, B.-C. and A.F.H. Goetz, Column atmospheric water vapor and vegetation liquid water retrievals from airborne imaging spectrometer, *J. Geophys. Res*., *95*, 3349-3564, 1990.

Giver, L.P., P. Pilewskie, W. J. Gore, C. Chackerian Jr., P. Varanasi, R.S. Freedman and R. Bergstrom, Uncertainties in the line Intensities in the 1130-nm band of water vapor, paper presented at ARM Science Team Meeting, Atmos. Radiat. Measure. Program,Atlanta, Ga., March, 2001.

Giver, L.P., C. Chackerian Jr., and P. Varanasi, Visible and near-infrared H_2O line intensity correction for Hitran-96, *J. Quant. Spectrosc. Radiat. Transfer*, *66*, 101-105, 2000.

Hansen, J.E., and L.D. Travis, Light scattering in planetary atmospheres, *Space Sci. Rev*., *16*, 527-610, 1974.

Harrison, L., J. Michalsky, and J. Berndt, Automated multifilter rotating shadow-band radiometer: an instrument for optical depth and radiation measurements, *Appl. Opt.*, *33*, 5118-5125, 1994.

Harrison, L., M. Beauharnois, J. Berndt, P. Kiedron, J. Michalsky, and Q. Min, The rotating shadowband spectroradiometer (RSS) at SGP, *Geophys. Res. Lett*., *26*, 1715-1718, 1999.

Ingold, T., B. Schmid, C. Matzler, P. Demoulin, and N. Kampfer, Modeled and empirical approaches for retrieving columnar water vapor from solar transmittance measurements on the 0.72, 0.82, and0.94-micrometer bands, *J. Geophys. Res.*, *105*, 24,327-24,343, 2000.

Kasten, F., A new table and approximation formula for relative air mass, *Arch. Meteorol. Geophys. Bioklimatol*., *Ser. B*, *14*, 206-223, 1965.

Kiedron, P.W., J.J. Michalsky, J.L. Berndt, and L.C. Harrison, Comparison of spectral irradiance standards used to calibrate shortwave radiometers and spectroradiometers, *Appl. Opt.*, *38*, 2432-2439, 1999.

Kneizys, F. X., et al., The Modtran 2/3 report and LOWTRAN 7 model, Phillips Lab., Geophys. Dir., Hanscom Air Force Base, Mass., Jan. 1996.

Lesht, B.M., Reanalysis of radiosonde data from 1996 and 1997 water vapor intensive observation periods: Application of the Vaisala RS-80H contamination correction algorithm to dual sonde soundings, paper presented at ARM Meeting, Atmos. Radiat. Measure. Program, San Antonio, Tex.,1999.

Liljegren, J. C., and B. M. Lesht, Measurements of integrated water vapor and cloud liquid water from microwave radiometers at the DOE ARM Cloud and Radiation Testbed in the U.S. Southern Great Plains, paper presented at the International Geoscience and Remote Sensing Symposium'96, Lincoln, Neb., 1996.

Liljegren, J., Automatic self-calibration of ARM microwave radiometers, in Microwave Radiometric Remote Sensing of Earth's Surface, edited by P. Pamploni and S. Paloscia, 2000.

Michalsky, J.J., Q. Min, and P. W. Kiedron, D. W. Slater and J. C. Barnard, A differential technique to retrieve column water vapor using sun radiometry, *J. Geophys. Res.*, in press, 2001.

Michalsky, J.J., L.C. Harrison, and W.B. Berkheiser, Cosine response characteristics of some radiometric and photometric sensors, *Sol. Energy*, *54*, 397-402, 1995.

Mlawer, E. J., P. D. Brown, S. A. Clough, L. C. Harrison, J. J. Michalsky, P. W. Kiedron, and T. Shippert, Comparison of spectral direct and diffuse solar irradiance measurements and calculations for cloud-free conditions, *Geophys. Res. Lett.*, *27*, 2653-2656, 2000.

Racette, P., R.F. Adler, J.R. Wang, A.J. Gasiewski, D.M. Jackson and D.S. Zacharias, A millimeter-wave imaging radiometer for cloud, precipitation and atmospheric water vapor studies, *J. Atmos. Oceanic Technol.*,*13*, 610-619, 1996.

Racette, P., E.R. Westwater, Y. Han, W. Manning, A. Gasiewski, and D.C Jones, Millimeter-wave measurements of low amounts of precipitable water vapor, paper presented at International Geoscience and Remote Sensing Symposium' 00, Honolulu, Hawaii, 2000.

Rosenkranz, P.W., Water vapor microwave continuum absorption: A comparison of measurements and models, *Radio Sci.*, *33*, 919-928, 1998.

Rothman, L. S., et al., The HITRAN molecular spectroscopic database and HAWKS (HITRAN AtmosphericWorkstation): 1996 Edition, *J. Quant. Spectrosc. Radiat. Transfer*, *60*, 665-710, 1998.

Schotland, R.M., and T.K. Lea, Bias in a solar constant determination by Langley method due to structured atmospheric aerosol, *Appl. Opt.*, *25*, 2486-2491, 1986.

Schmid, B., K.J. Thome, P. Demoulin, R. Peter, C. Matzler, and J. Sekler, Comparison of modeled and empirical approaches for retrieving columnar water vapor from solar transmittance measurements in the 0.94 μm region, *J. Geophys. Res.*, *101*, 9345-9358, 1996.

Stokes, G.M., and S.E. Schwartz, The atmospheric radiation programmatic background and design of the cloud and radiation test bed, *Bull. Am. Meteorol. Soc*., *75*, 1201-1221, 1994.

Thome, K.J., B.H. Herman, and J.A. Reagan, Determination of precipitable water from solar transmission, *J. Appl. Meteorol.*, *31*, 157-165, 1992.

Wade, C. G., An evaluation of problems affecting the measurementof low relative humidity on U.S. radiosonde, *J. Atmos. Oceanic Technol.*, *11*, 687-700, 1994.

Westwater, E.R., B.B. Stankov, Y. han, J.A. Shaw, C.N. Long, B.M. Lesht and J. Shannahoff, Comparison of microwave radiometers and radiosondes during Nauru-99 experiment, paper presented at International Geoscience and Remote Sensing Symposium' 00, Honolulu, Hawaii, 2000a.

Westwater, E.R., Y. Han, P.E. Racette, W. Manning, A. Gasiewski, and M. Klein, A comparison of clear-sky emission models with data taken during the 1999 Millimeter-Wave Radiometric Arctic Winter Water Vapor Experiment, paper presented at ARM Science Team Meeting, Atmos. Radiat. Measure. Program, San Antonio, Tex., 2000b.

_____

J. Berndt, L. Harrison, P. Kiedron, J. Michalsky, ASRC, State University of New York at Albany, 251 Fuller Road, Albany, NY 12203,USA. (kiedron@asrc.cestm.albany.edu**)**

Y. Han and E, Westwater, CIRES, University of Colorado, 325 Broadway MS R/E/ET1,Boulder, Colorado 80305 CO, USA. (Ed.R.Westwater@noaa.gov)

P. Racette, NASA Goddard Space Flight Center, Microwave Instrument Technology Branch, Code 555, Building 19, Room N15, Greenbelt, MD 20771, USA. (per@priam.gsfc.nasa.gov)

B. Schmid, Bay Area Environmental Research Institute, NASA Ames Research Center, MS 245-5, Moffett Field, CA 94035-1000, USA. (bschmid@mail.arc.nasa.gov)

D. Slater, Pacific Northwest National Laboratory, P.O. Box 999, K9-55, Richland, WA 99352, USA. (donald.slater@pnl.gov)

(received November 6, 2000; revised May 22, 2001;
accepted May 23, 2001.)

Paper number 2000JD000130.
0148-0227/01/2000JD000130$09,00

Table 1. Statistical Summary of Comparison of Rotating Shadowband Spectroradiometer (RSS) Retrievals With Microwave Radiometer (MWR) and Millimeter Wave Imaging Radiometer (MIR) Retrievals for Eight Days in March 1999.

	Correlation Coefficient	Average Difference, mm	RMS Difference, mm	Intercept, mm	Slope
MWR -RSS	0.956	0.298	0.304	-0.135	0.895
MIR±3 -RSS	0.948	-0.205	0.232	0.046	1.134
MIR±7 -RSS	0.968	0.120	0.145	-0.090	0.979

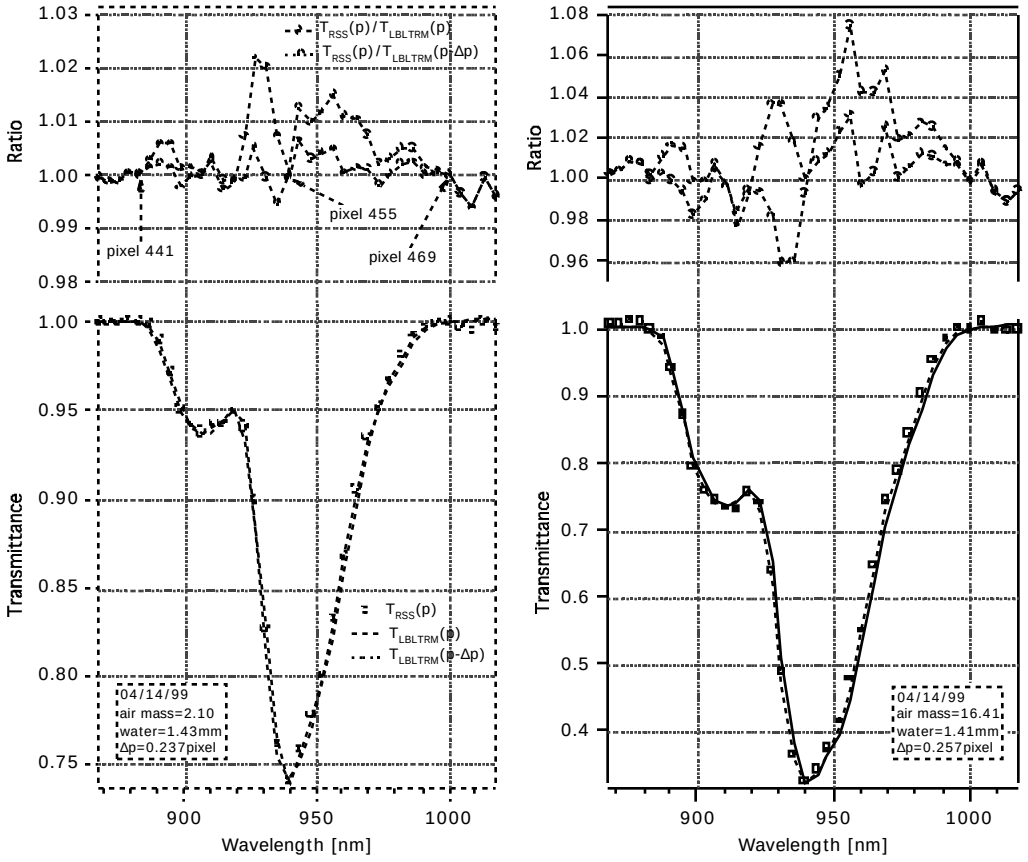

Figure 1. Comparison of measured and model transmittance at 37 pixels surrounding the 940-nm water vapor absorption band at two different air masses. The model transmittance was obtained with two methods: the first (continuous line) matches measured transmittance at pixel 455, and the second (dashed line) allows the wavelength shift to minimize rms error at three pixels: 454, 455, and 456 near the maximum absorption in this band.

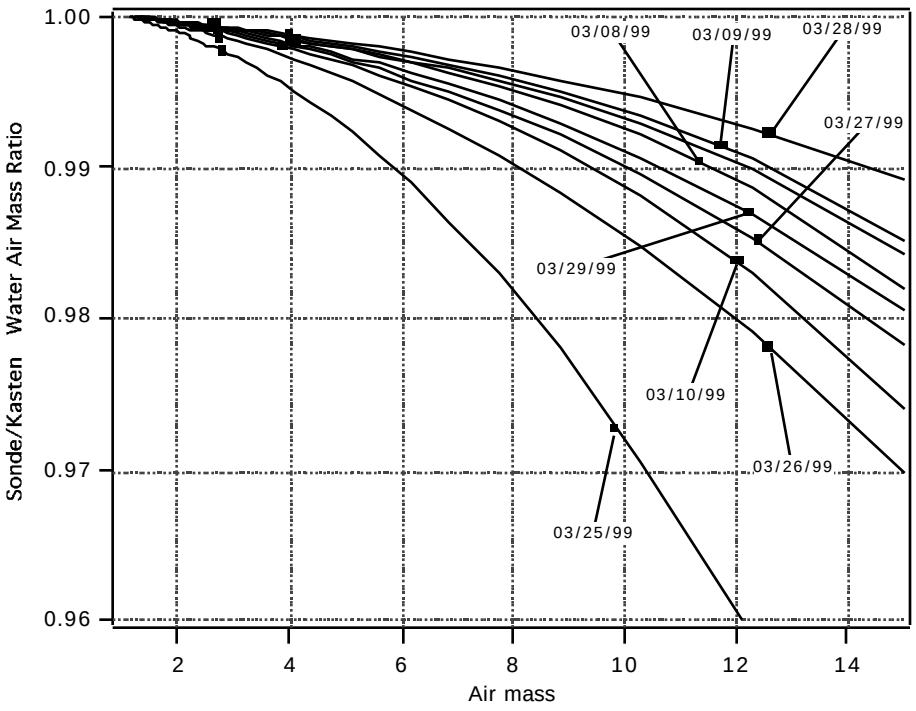

Figure 2. Ratio of water vapor air mass obtained from radiosonde water vapor column profiles to water vapor air mass from(10). The markers on each curve indicate the range of air masses within which rotating shadowband spectroradiometer (RSS) retrievals were performed.

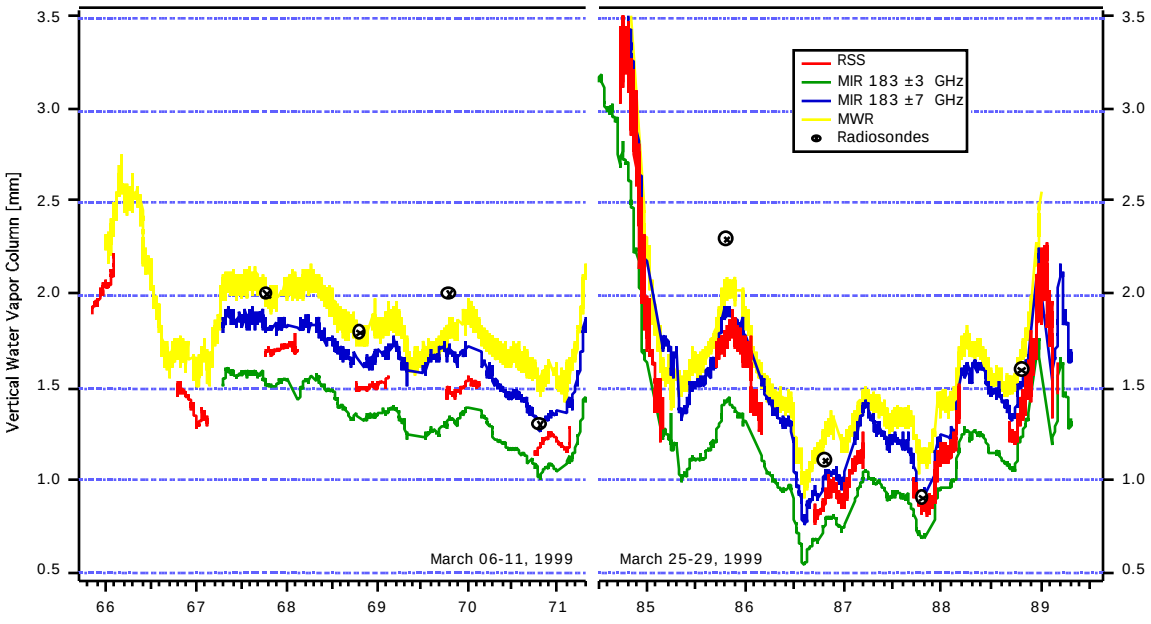

Plate 1. RSS retrievals are compared with results from three microwave radiometer measurements and radiosonde results.

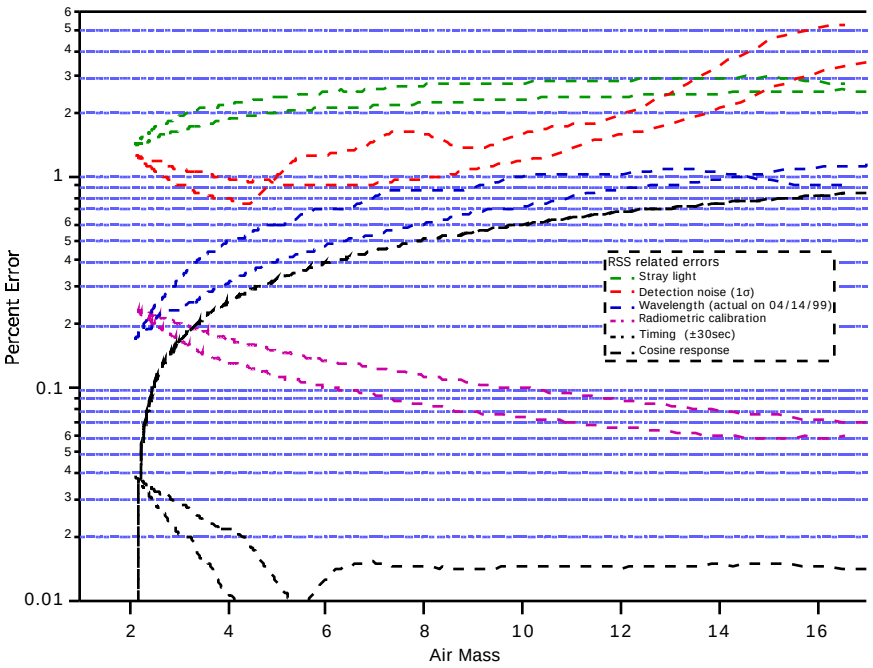

Plate 2. Estimates of errors related to aspects of measurement with the RSS are presented here for the retrieval on April 14, 1999.

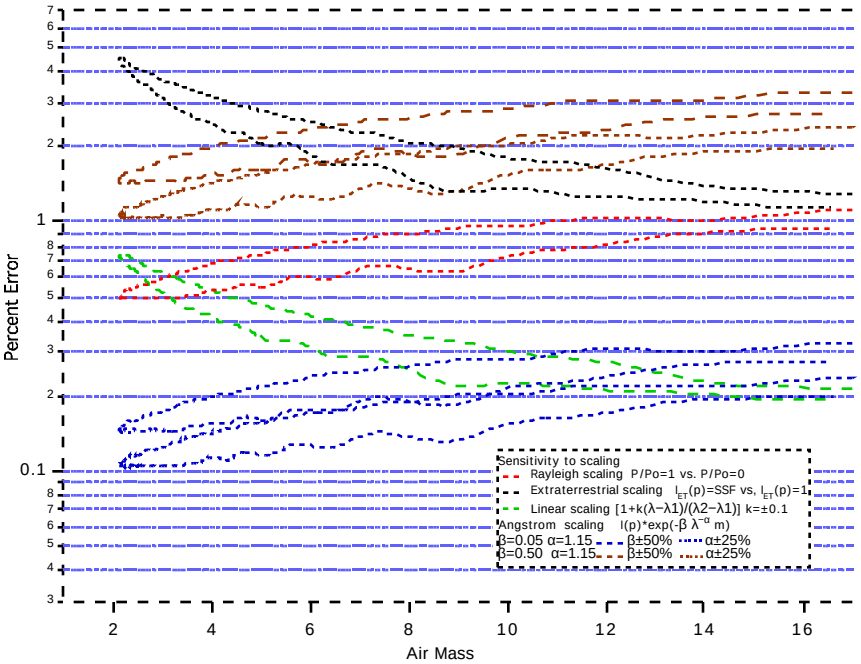

Plate 3. Results of simulations to evaluate the method's robustness for the retrieval on April 14, 1999.